Fractionation of Ne and Ar isotopes by molecular diffusion in water

Lina Tyroller[a,b,*], Matthias S. Brennwald[a], Lars Mächler[a], David M. Livingstone[a], Rolf Kipfer[a,b,c]

[a] *Eawag, Swiss Federal Institute of Aquatic Science and Technology, Dübendorf, Switzerland*
[b] *ETH Zurich, Institute of Biogeochemistry and Pollutant Dynamics, Zürich, Switzerland*
[c] *ETH Zurich, Institute of Geochemistry and Petrology, Zürich, Switzerland*

Abstract

Molecular diffusion in water is a physical transport mechanism that plays an important role in many environmental processes. As the abundances of the chemically inert noble gases and their isotopes are controlled only by physical processes, they are ideal tracers for gas transfer processes in aquatic systems. Molecular diffusion in water is often thought to cause the mass-dependent fractionation of noble gas isotope ratios, e.g. ^{20}Ne/^{22}Ne and ^{36}Ar/^{40}Ar, under the assumption that the isotopic fractionation of gases in water can be adequately described in terms of a "square root relation", i.e. in terms of the reciprocal of the square root of the ratio of their atomic masses. To quantify reliably the fractionation of ^{20}Ne/^{22}Ne and ^{36}Ar/^{40}Ar we determined the change in the isotope ratios of Ne and Ar after they had diffused through immobilised water. The Ne isotope fractionation factor, expressed as the ratio of the diffusion coefficients of ^{20}Ne and ^{22}Ne, was found to be $D_{^{20}\mathrm{Ne}}/D_{^{22}\mathrm{Ne}} = 1.010 \pm 0.003$, which is considerably lower than that predicted

*Corresponding author
Email addresses: lina.tyroller@eawag.ch (Lina Tyroller), matthias.brennwald@eawag.ch (Matthias S. Brennwald), lars.maechler@eawag.ch (Lars Mächler), living@eawag.ch (David M. Livingstone), kipfer@eawag.ch (Rolf Kipfer)

from the square root relation, but close to results obtained from recent molecular dynamics calculations. In contrast to this, the Ar isotopic fractionation factor was found to be $D_{^{36}Ar}/D_{^{40}Ar} = 1.055 \pm 0.004$, agreeing with that predicted from the square root relation. Thus, neither the square root relation nor calculations based on molecular dynamics are capable of giving a general explanation of the isotopic fractionation of both Ne and Ar that results when these gases undergo molecular diffusion through water. Our experimental results do not rely on a theoretical model and are considered to provide an accurate and robust quantification of the isotopic fractionation of Ne and Ar isotopes induced by molecular diffusion through water.

Keywords: Graham's Law, noble gases, kinetic fractionation, isotope ratio, excess air

1. Introduction

Noble gases and their isotopes are used as environmental tracers in aquatic systems because of their sensitivity to the transport and exchange of solutes and fluids. Noble-gas concentration patterns in natural water bodies have been successfully used to reconstruct palaeoclimates, to analyse circulation and mixing within water bodies, to quantify water residence times and to study the geochemical origin of fluids injected into water bodies (for reviews see Kipfer et al., 2002; Schlosser and Winckler, 2002; Aeschbach-Hertig and Solomon, 2013; Brennwald et al., 2013)

Molecular diffusion in water is commonly expected to result in the elemental fractionation of noble gases and in the fractionation of the ratios of noble gas

isotopes owing to systematic differences in their diffusion coefficients (e.g., Ozima and Podosek, 2002). The fractionation of the isotope ratios of noble gases dissolved in water (e.g. $^{20}Ne/^{22}Ne$ and $^{36}Ar/^{40}Ar$) has been used to assess the importance of molecular diffusion for various environmental processes, such as: (I) transport in pore water; (II) degassing in supersaturated pore water; and (III) the dynamics of excess air in groundwater.

I. If the transport of noble gases in pore water (e.g. in lake sediments) is controlled by molecular diffusion, the noble-gas isotope ratios in the pore water would be expected to be fractionated relative to the noble-gas isotope ratios found in air-saturated water. If the transport of noble gases in the sediment is dominated by advection, however, no fractionation would be expected.

II. Bubble formation and degassing generally results when the partial pressure of dissolved gases in the pore water exceeds the in situ pressure. In environmental systems such as lake sediments (Brennwald et al., 2003, 2005, 2013) and groundwater (for a review see Aeschbach-Hertig et al., 2008), patterns in the concentrations of dissolved noble gases are used to trace the formation of bubbles generated by biological processes (e.g. the production of CO_2 or CH_4). The difference of the partial pressure of the gases in the bubble and in the surrounding water results in the diffusion of noble gases from the water into the bubbles. If the bubbles remain in the water until gas exchange between the bubbles and the surrounding water reaches steady

state, the gas partitioning is controlled by the solubilities of the gases. This results in the elemental fractionation of the noble gases in the surrounding water, but in virtually no isotopic fractionation. If the bubbles leave the water before steady state is attained, the noble-gas isotope ratios are assumed to be fractionated relative to air-saturated water (Lippmann et al., 2003; Brennwald et al., 2005; Zhou et al., 2005; Klump et al., 2006; Visser et al., 2007).

III. Excess air results from the entrapment of air bubbles in groundwater. Owing to the increasing hydrostatic pressure during groundwater recharge, the entrapped bubbles dissolve, leading to the higher noble-gas concentrations (relative to air-saturated water) that are characteristic of groundwater. The formation of excess air has been explained using various different conceptual models (for a review see Schlosser and Winckler, 2002; Aeschbach-Hertig and Solomon, 2013). Molecular diffusion plays a role in models that describe the partial re-equilibration of excess air in groundwater with the atmosphere. Part of the excess air diffuses through the groundwater body and to the soil gas of the unsaturated zone. The isotope ratios $^{20}Ne/^{22}Ne$ and $^{36}Ar/^{40}Ar$ have therefore been suggested as tools to determine which of the different conceptual models for excess-air formation is likely to be most correct (Holocher et al., 2002; Kipfer et al., 2002; Peeters et al., 2002; Aeschbach-Hertig and Solomon, 2013). This is important because these conceptual models are necessary when using noble-gas concentrations to reconstruct the environmental conditions that prevailed during groundwater

recharge.

All the above-mentioned applications of noble-gas isotope ratios in aquatic systems to interpret noble gas concentration patterns in terms of physical gas transport processes rely on a parameterisation of the diffusion rates in terms of the reciprocal of the square root of the atomic mass of the gas. This "square root relation" is implicitly derived from Graham's Law (Graham, 1833), which describes the fractionation of two gas species undergoing diffusion in a gaseous matrix for the case where collisions between different gas molecules are rare and pressure is constant (Schwarzenbach et al., 2003; Cussler, 2009). Because Graham's Law and the square root relation derived from it are both ultimately based on kinetic gas theory (Moore, 1999), they lack the theoretical basis that would allow their application to the diffusion of solutes through water.

The square root relation can be stated in the following form (e.g. Richter et al., 2006) :

$$\frac{D_i}{D_j} = \sqrt{\frac{M_j}{M_i}} \tag{1}$$

where D_i and D_j are the diffusion coefficients of the diffusing gases i and j, and M_i and M_j are their molecular masses. If gas-gas collisions are more frequent, however, the square root relation is modified by introducing the reduced masses μ_i and μ_j of the diffusing gases (e.g. Craig and Gordon, 1965; Richter et al., 2006):

$$\frac{D_i}{D_j} = \sqrt{\frac{\mu_j}{\mu_i}} \qquad \text{with } \mu_i = \frac{M_i M_{\mathrm{ma}}}{M_i + M_{\mathrm{ma}}} \text{ and } \mu_j = \frac{M_j M_{\mathrm{ma}}}{M_j + M_{\mathrm{ma}}} \tag{2}$$

where M_{ma} is the molecular mass of the matrix gas through which comparatively low concentrations of gases i and j with molecular masses M_i and M_j, respectively, are diffusing.

Recent molecular dynamics calculations (Bourg and Sposito, 2008) have challenged the applicability of the square root relation for characterizing the isotopic fractionation of dissolved noble-gas isotopes by molecular diffusion in water. Bourg and Sposito (2008) simulated the diffusion of different noble gases and their isotopes in water on an atomic scale, predicting their behaviour by assuming theoretical intermolecular potential functions. Their results suggest a more general power-law form of Eq. 1:

$$\frac{D_i}{D_j} = \left(\frac{M_j}{M_i}\right)^{\beta} \tag{3}$$

in which $0 < \beta < 0.2$ rather than the expected value of $\beta = 0.5$.

Experimental data on the fractionation of noble gases by molecular diffusion in water are scarce. Jähne et al. (1987a) measured the elemental diffusivities of He, Ne, Kr, Xe and Rn in water and found them to be consistent with the square root relation (Eq. 1). In their experiments, gas diffuses from a gas-filled chamber through a diffusion cell containing immobilised water into another chamber. The advantage of this experimental approach is that the system can be described with a single diffusion equation (Schwarzenbach et al., 2003; Cussler, 2009) that can be fitted to the experimental data. However this approach has not yet been used to determine the fractionation of the isotopes of a single noble-gas species.

To date the only experimental data available on the kinetic isotopic fractionation of noble-gas isotopes in water have been based on air/water gas exchange models, where mass transfer at the gas/water interface is related to diffusion (for a review see Cussler, 2009). Jähne et al. (1987a) studied gas/water mass transfer in an evasion experiment with a circular wind-wave facility and concluded that the isotopic fractionation of He was consistent with the square root relation. A recent study (Tempest and Emerson, 2013) determined gas/water mass transfer for Ne and Ar in a system in which the gas headspace was connected to degassed water. In this experiment, the isotopic fractionation observed was weaker than that predicted by the square root relation, but similar to that predicted by the molecular dynamics model of Bourg and Sposito (2008). However, the setup used in these studies was designed to study the transfer of gases across the thin boundary layers of the air/water interface in natural surface waters, and this is affected by large -scale mixing on both sides of the interface (Jähne et al., 1987b). The quantitative relationship between the gas-exchange rates obtained in such mass-transfer experiments and the diffusion coefficients of the gases involved depends on the choice of a suitable gas-exchange model (Schwarzenbach et al., 2003; Cussler, 2009). Combining an empirical gas-exchange model for natural waters with gas-transfer rates obtained in an artificial laboratory experiment with considerably different turbulence levels in the boundary layers does not provide a direct measurement of the isotopic fractionation resulting from molecular diffusion in water.

Instead of a ”mass transfer approach”, in this study a ”diffusion approach” is used in which the diffusive transport of gases through immobilised water can

be expressed by a single diffusion equation. To our knowledge this is the first time that the isotopic fractionation of noble gases has been measured based on a diffusion approach using an experimental setup similar to the modified Barrer method used by Jähne et al. (1987a). We determined directly the fractionation of $^{20}Ne/^{22}Ne$ and $^{36}Ar/^{40}Ar$ resulting from molecular diffusion in bulk water and measured the relative differences of the isotope fluxes through a diffusion column containing immobilised water. We compare our experimentally measured isotopic fractionation with the two versions of the square root relation (Eqs. 1, 2) and molecular dynamics calculations (Eq. 3) to evaluate the applicability of each.

2. Material and methods

2.1. Experimental setup

Our setup (Fig. 1) consisted of a diffusion column comprising two gas-filled chambers, A and B, separated by a diffusion cell. Before the start of the experiment, both chambers were flushed with carrier gas (N_2 of 99.999% purity, Carbagas, Switzerland) to remove residuals of other gases from the apparatus. During the experiment, chamber A was continuously flushed with one of the test gases (Ne or Ar of 99.999% purity, Carbagas, Switzerland; gas flow: $8 cm^3_{STP}/min$) and chamber B with the carrier gas (N_2 gas flow: $4 cm^3_{STP}/min$). The difference in the partial pressure of the test gas between A ($\sim$ 1 atm) and B ($\sim$ 0 atm) meant that some of the test gas diffused through the diffusion cell from chamber A to chamber B. The test gas reaching chamber B was flushed out together with the carrier gas. To prevent turbulent transport within the diffusion cell, the water in the diffu-

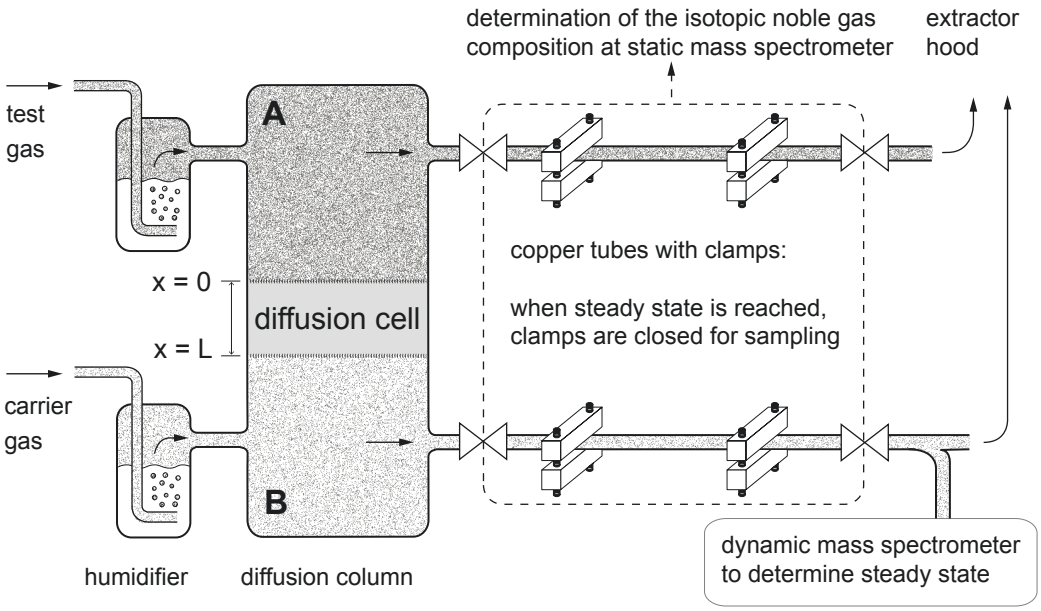

Figure 1: Experimental setup. During the experiment both temperature and pressure were kept constant. A test gas and a carrier gas are flushed continuously through two chambers (A and B, respectively) separated by a diffusion cell containing an agar-water gel. All fittings, valves and connection tubes are gas-tight and made of stainless steel or copper. Desiccation of the agar-water gel in the diffusion cell, which might result in cracks, is prevented by bubbling the gases through pure water in humidifiers to saturate them with water vapour before they are injected into the gas-filled chambers. Bacterial growth in the diffusion cell is inhibited by adding 0.01% NaN_3 to the gel. The outflowing gases are discharged into an extractor hood. The gas-carrying outlet tubes are always open to ambient air at local atmospheric pressure.

sion cell was immobilised by adding 0.5% agar (porosity 99%) as recommended by Jähne et al. (1987a). The agar-water gel lay on a glass frit (porosity 42%). Repeated experiments were carried out using different gel thicknesses (L =1.7-2.0 cm, see Tab. 1). Turbulent mixing can be assumed to result in homogeneously mixed gases in chambers A and B, making additional mechanical homogenisation unnecessary.

The carrier gas flowing out of chamber B was continuously analysed and mon-

itored with a quadrupole mass spectrometer operated in dynamic mode (Mächler et al., 2012) to assess the performance of the experimental apparatus and to determine when the gas flux through the diffusion cell had attained steady state. These measurements were not used to determine the $^{20}Ne/^{22}Ne$ and $^{36}Ar/^{40}Ar$ ratios because of interference resulting from doubly charged ions and matrix effects, which strongly limits the precision of the noble-gas analysis (see Mächler et al., 2012). When the continuous measurements indicated that the test-gas flux through the diffusion cell had attained steady state, samples of the gases flowing out of chambers A and B were taken in copper tubes for isotope-ratio analysis by static mass spectrometry (Beyerle et al., 2000). In brief, the gas samples were separated into a He-Ne fraction and an Ar-Kr-Xe fraction using a series of cryogenic traps. These gas fractions were then purified using additional cryogenic traps, zeolite traps and getter traps, which removed any reactive gases. The purified noble gases were then analysed in a custom-built, sector-field mass spectrometer by peak-height comparison relative to an air standard processed using exactly the same procedure as that used for the sample gas.

2.2. Principles of the measuring method

After switching on the flow of test gas through chamber A, the test gas starts to diffuse through the diffusion cell. In an initial, non-steady-state phase, the test-gas flux through the diffusion cell increases until it eventually attains steady state.

2.2.1. Non-steady state

By differentiating Eq. 4.24a of Crank (1975) with respect to time, the time-dependent diffusive flux $F_i(t)$ of the test-gas species i from the diffusion cell into chamber B can be calculated as follows:

$$F_i(t) = \frac{D_i C_i(0)}{L}\left(1 + 2\sum_{n=1}^{\infty}(-1)^n \exp\left(-D_i n^2 \pi^2 \frac{t}{L^2}\right)\right) \quad (4)$$

where t is time ($t = 0$ at the start of the experiment, when chamber A is completely flushed by the flow of test gas); D_i is the diffusion coefficient of species i in the diffusion cell; and $C_i(x)$ is the concentration of species i in the diffusion cell at position x ($x = 0$ at the top of the diffusion cell and $x = L$ at the bottom; see Fig. 1). The assumptions underlying Eq. 4 are that $C_i(0 \leq x \leq L) = 0$ for $t < 0$; that $C_i(0) > 0$ and is time-independent for $t \geq 0$, and that $C_i(L) \ll C_i(0)$ for $t \geq 0$. The breakthrough time T (the characteristic time required for F_i to undergo a substantial increase) is given by Eq. 4.26 of Crank (1975):

$$T = \frac{L^2}{6D_i} \quad (5)$$

2.2.2. Steady state

The gas flux $F_i(t)$ from the diffusion cell into chamber B is considered to have attained steady state when $t \gtrsim 3T$ (Daynes, 1920; Crank, 1975). Eq. 4 can then be simplified to:

$$F_i = D_i \frac{C_i(0)}{L} \quad (6)$$

The isotopic fractionation factor for two different species i and j – i.e., the ratio of their diffusion rates or, equivalently, of their diffusion coefficients – can be obtained from the concentration ratio $R^0_{i,j} = C_i(0)/C_j(0)$ at the upper interface of the diffusion cell and the flux ratio $R^L_{i,j} = C_i(L)/C_j(L) = F_i/F_j$ at the lower interface of the diffusion cell, according to Eq. 6:

$$\frac{R^L_{i,j}}{R^0_{i,j}} = \frac{F_i/F_j}{C_i(0)/C_j(0)} = \frac{D_i}{D_j} \tag{7}$$

Note that the isotopic fractionation of Ne and Ar at solubility equilibrium in water is very small (see Beyerle et al., 2000). If i and j are two isotopes of the same element, $R^0_{i,j}$ can therefore be assumed to be identical to the isotope concentration ratio in the pure test gas flowing through chamber A, and $R^L_{i,j}$ can be assumed to be identical to the concentration ratio of the two isotopes in the carrier gas leaving the system via chamber B. We were therefore able to determine the isotope fractionation factor from Eq. 7 simply by measuring the isotope ratios in chambers A and B using static mass spectrometry. The advantage of this approach is that quantification of the fractionation factor is virtually independent of the geometry of the diffusion column, as it relies only on the isotope concentration ratios in chambers A and B, which can be measured precisely and straightforwardly using a standard noble-gas analysis protocol (Beyerle et al., 2000).

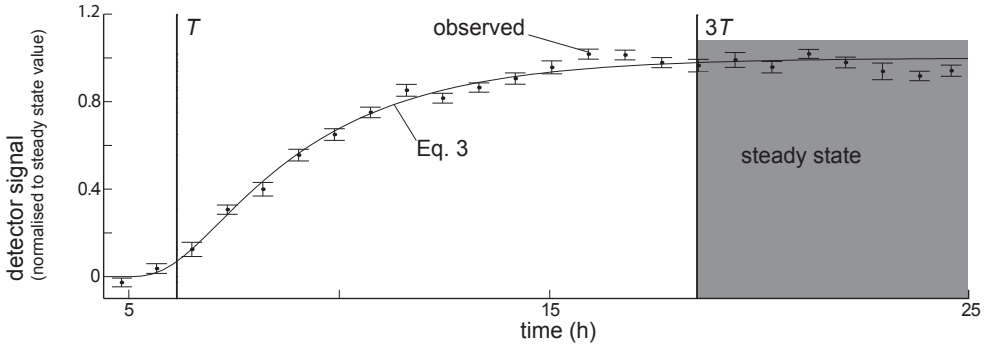

Figure 2: Breakthrough curves of ^{20}Ne. Dots indicate "observed" data, measured in the outlet of chamber B with a quadrupole mass spectrometer (error bars indicate standard errors). The curve shown is the theoretical breakthrough curve, calculated from Eq. 4 with $D_{^{20}\mathrm{Ne}} = 3.0 \times 10^{-9}\,\mathrm{m}^2\,/\mathrm{s}$ (Wise and Houghton, 1968) and $L = 2.0\,\mathrm{cm}$. The breakthrough time $T = 6.2\,\mathrm{h}$ was calculated from Eq. 5 based on the same values for $D_{^{20}\mathrm{Ne}}$ and L. Steady state is considered to be attained at time $3T$ (Daynes, 1920; Crank, 1975).

3. Results and discussion

3.1. Experiment performance

Fig. 2 shows the observed and theoretical breakthrough curves calculated using Eq. 4. The curves are in excellent agreement, as are the breakthrough times, indicating that the experiment performs exactly as would be expected based on the description given above (Sect. 2.2). By inserting the isotope ratios measured in chambers A and B into Eq. 7, an accurate quantification of the isotopic fractionation resulting from diffusive transport through the diffusion cell can therefore be obtained.

3.2. Fractionation factors

The flux of the test gas through the diffusion cell attained steady state approximately 18 h after the start of the experiment ($3T$ in Fig. 2). ^{20}Ne/^{22}Ne and

Table 1: $^{20}Ne/^{22}Ne$ and $^{36}Ar/^{40}Ar$ ratios and their standard errors measured in chambers A and B at steady-state conditions in different experimental runs (2 runs with Ne, 4 runs with Ar) using diffusion cells with different thicknesses L.

	$^{20}Ne/^{22}Ne$	$^{36}Ar/^{40}Ar \times 10^{-3}$
	Chamber A ($R^0_{i,j}$)	
Test gas (dry):	9.76 ± 0.02	3.36 ± 0.01
Test gas (humidified):	9.76 ± 0.02	3.36 ± 0.01
Mean, error of the mean:	9.76 ± 0.02	3.36 ± 0.01
	Chamber B ($R^L_{i,j}$)	
L = 1.7 cm	9.86 ± 0.02	3.54 ± 0.01
L = 1.7 cm	—	3.54 ± 0.01
L = 2.0 cm	9.86 ± 0.02	3.54 ± 0.01
L = 2.5 cm	—	3.56 ± 0.01
Mean, error of the mean:	9.86 ± 0.02	3.545 ± 0.006

$^{36}Ar/^{40}Ar$ ratios measured in the test gas leaving chamber A were equal to the ratios measured in the test gas before it passed through the humidifier. The results of different replicate experiments are given in Tab. 1. $^{20}Ne/^{22}Ne$ and $^{36}Ar/^{40}Ar$ ratios were measured at steady state in chambers A and B. For the Ne test gas in chamber A the measured isotope ratio was slightly lower than in air ($^{20}Ne/^{22}Ne$ = 9.80; Ozima and Podosek, 2002), which is consistent with the findings of Pavese et al. (2005) that purified atmospheric Ne from different commercial sources tends to be enriched in ^{22}Ne. The $^{36}Ar/^{40}Ar$ ratio in the test gas in chamber A showed no fractionation relative to the $^{36}Ar/^{40}Ar$ ratio of air ($^{36}Ar/^{40}Ar = 3.384 * 10^3$; Ozima and Podosek, 2002). Note that for consistency with previous data measured in our noble gas laboratory we used the $^{36}Ar/^{40}Ar$ value of Ozima and Podosek

(2002) (as recommended by the IUGS Subcommission on Geochronology) rather than the more recent values reported by Lee et al. (2003) and Mark et al. (2011).

For both the $^{20}Ne/^{22}Ne$ and $^{36}Ar/^{40}Ar$ ratios the results obtained from the individual replicate gas samples agreed to within their respective standard errors. In agreement with the theory, the ratios determined were found to be independent of the thickness of the diffusive layer (Tab. 1). Diffusion through the diffusion cell resulted in increases of 1.0 ±0.3% and 5.5 ±0.4%, respectively, in the experimentally observed $^{20}Ne/^{22}Ne$ and $^{36}Ar/^{40}Ar$ ratios.

Tab. 2 lists the fractionation factors calculated from Eq. 7 using the mean values of the $^{20}Ne/^{22}Ne$ and $^{36}Ar/^{40}Ar$ ratios measured in chambers A and B (Tab. 1) and compares the experimentally determined isotopic fractionation with the isotopic fractionation predicted by the square root relation (Eq. 1), by the modified square root relation (Eq. 2) and by the results of the molecular dynamics simulation of Bourg and Sposito (2008) (Eq. 3). Our experimentally determined $^{20}Ne/^{22}Ne$ fractionation factor is significantly smaller than that calculated from the square root relation (Eq. 1), but agrees with the predictions based on the molecular dynamics calculations of Bourg and Sposito (2008), (Eq. 3). In contrast to this, our experimentally determined $^{36}Ar/^{40}Ar$ fractionation factor agrees with that calculated from the square root relation (Eq. 1), but *not* with that based on the molecular dynamics calculations. The $^{20}Ne/^{22}Ne$ and $^{36}Ar/^{40}Ar$ fractionation factors predicted by the modified square root relation (Eq. 2) are inconsistent with all our experimental results.

Note that the $^{20}Ne/^{22}Ne$ and $^{36}Ar/^{40}Ar$ fractionation factors inferred from the

Table 2: Comparison of fractionation factors determined experimentally in this study with fractionation factors determined from the square root relation or molecular dynamics calculations (including standard errors; the 2σ errors reported by Bourg and Sposito (2008) were converted to 1σ errors) and from the square root relation*, treating water as if it were a gas of molecular weight 18.

	$D_{^{20}Ne}/D_{^{22}Ne}$	$D_{^{36}Ar}/D_{^{40}Ar}$
This study (from means in Tab. 1)	1.010 ± 0.003	1.055 ± 0.004
Square root relation (Eq. 1)	1.049	1.054
Modified square root relation* (Eq. 2)	1.022	1.017
Molecular dynamics (Bourg and Sposito, 2008) (Eq. 3)	1.014 ± 0.001	1.008 ± 0.002

square root relation (Eq. 1) are very similar, because the mass ratios of the two isotope pairs are almost the same ($20/22 \approx 0.909$ and $36/40 \approx 0.900$). This close agreement is in contrast to the difference in the fractionation behaviour of the Ne and Ar isotopes observed in our experiments. It is possible that this discrepancy results from the fact that square root relation is based on the kinetics of diffusion in gases rather than in water. We also note that for Ar, the results of the molecular dynamics calculations of Bourg and Sposito (2008) are not consistent with the experimental results of our study. As pointed out by the authors, the accuracy of the molecular dynamics calculations is limited by our knowledge of the intermolecular potential functions used in the model.

Therefore, and because the results obtained from the modified square root relation (Eq. 2) are also inconsistent with the experimental results, neither of the forms of the square root relation nor the molecular dynamics simulation would seem to provide an adequate, generally valid, physically sound description of the isotopic fractionation of both Ne and Ar that results from molecular diffusion in water.

However, our results do provide clear evidence that the square root relation is able to describe adequately the isotopic fractionation of $^{36}Ar/^{40}Ar$. Arguments on the transport of dissolved substances in water by molecular diffusion that are based primarily on the $^{36}Ar/^{40}Ar$ ratio (e.g., Peeters et al., 2002; Brennwald et al., 2005) therefore remain valid and can still be used to determine whether molecular diffusion controls noble gas abundances in natural water, as the assumed behaviour of the Ar isotopes is consistent with our newly determined isotopic fractionation factor.

We hypothesize that different intermolecular forces between noble gases and dipole water molecules might explain our experimental findings. This hypothesis is supported by quantum-chemical calculations supplemented by structural parameters describing the geometry of noble gas-water complexes in liquid water (Bagno, 1998; Sun et al., 2013), with water molecules clustering around dissolved noble gases as a result of intermolecular interactions (Ludwig, 2001). Bagno (1998) found the intermolecular force between Ne and liquid water to be 40–60% lower than that between Ar and liquid water. A recent study by Sun et al. (2013) found the geometry of the Ne-(liquid)water complex to differ from the geometry of the Ar-(liquid)water, Kr-(liquid)water and Xe-(liquid)water complexes. In Ne-(liquid)water complexes, Ne is orientated away from the hydrogen bonds, implying that the internal rotation of the H_2O molecule is hindered less than in the case of Ar, Kr and Xe, which are orientated towards the hydrogen bonds. Sun et al. (2013) also found that the prevailing geometry of Ne-water complexes was almost the same for ^{20}Ne and ^{22}Ne, and concluded therefore that the isotopic effect

on the structures of the Ne-water complex was small. These findings might establish a conceptual framework for understanding why diffusive transport through water fractionates Ne and Ar isotopes differently.

4. Conclusions

We empirically quantified the fractionation of $^{20}Ne/^{22}Ne$ and $^{36}Ar/^{40}Ar$ ratios in response to the molecular diffusion of Ne and Ar in water. For $^{20}Ne/^{22}Ne$ the experimentally determined fractionation factor ($D_{^{20}Ne}/D_{^{22}Ne} = 1.010 \pm 0.003$) agrees well with the results of the molecular dynamics calculations of Bourg and Sposito (2008) ($D_{^{20}Ne}/D_{^{22}Ne} = 1.014 \pm 0.001$). However, it is significantly lower than that predicted either by the square root relation, Eq. 1 ($D_{^{20}Ne}/D_{^{22}Ne} = 1.049$) or the modified square root relation with reduced masses, Eq. 2 ($D_{^{20}Ne}/D_{^{22}Ne} = 1.022$).

By contrast, for $^{36}Ar/^{40}Ar$, the experimentally determined fractionation factor ($D_{^{36}Ar}/D_{^{40}Ar} = 1.055 \pm 0.004$) agrees well with that predicted by the square root relation ($D_{^{36}Ar}/D_{^{40}Ar} = 1.054$) (implying that models relying on this relationship remain valid). However, it is significantly higher than that predicted either by the modified square root relation ($D_{^{36}Ar}/D_{^{40}Ar} = 1.017$) or by the molecular dynamics calculations of Bourg and Sposito (2008) ($D_{^{36}Ar}/D_{^{40}Ar} = 1.008 \pm 0.003$).

Thus, neither the square root relation nor the molecular dynamics approach of Bourg and Sposito (2008) is capable of giving a general explanation of our experimental results for the fractionation of both $^{20}Ne/^{22}Ne$ and $^{36}Ar/^{40}Ar$. We speculate that the different fractionation behaviour of $^{20}Ne/^{22}Ne$ and $^{36}Ar/^{40}Ar$ in

water is related to intermolecular interactions between water molecules in the liquid phase and dissolved noble gases (Bagno, 1998; Sun et al., 2013). To expand our knowledge of the molecular diffusion of noble gas isotopes, we suggest measuring the isotopic fractionation resulting from diffusion for all noble gases and their isotopes in water and in other liquids with different physico-chemical properties (e.g., oils or alcohols). Despite the lack of a theoretical model that is able to explain quantitatively the fractionation factors determined in our experiments, we consider that our direct measurements provide a robust basis for studies that use the fractionation of the noble-gas isotope ratios ^{20}Ne/^{22}Ne and ^{36}Ar/^{40}Ar to assess molecular diffusion in water bodies.

Acknowledgements

This work was financed by the Swiss National Science Foundation (SNF-project 200020 – 132155). We thank Frank Richter and an anonymous reviewer for their helpful criticism, which greatly helped in improving the manuscript.

References

Aeschbach-Hertig, W., El-Gamal, H., Wieser, M., and Palcsu, L. (2008). Modeling excess air and degassing in groundwater by equilibrium partitioning with a gas phase. *Water Resour. Res.* **44**, 1–12.

Aeschbach-Hertig, W. and Solomon, D. (2013). Noble Gas Thermometry in Groundwater Hydrology. In *The Noble Gases as Geochemical Tracers*. Springer, Berlin, Heidelberg, pp. 81–122.

329 Bagno, A. (1998). The ab initio neon-water potential-energy surface and its re-
330 lationship with the hydrophobic hydration shell. *J. Chem. Soc. Faraday Trans.*
331 **94**, 2501–2504.

332 Beyerle, U., Aeschbach-Hertig, W., Imboden, D. M., Baur, H., Graf, T. and
333 Kipfer, R. (2000). A mass spectrometric system for the analysis of noble gases
334 and tritium from water samples. *Environ. Sci. Technol.* **34**, 2042–2050.

335 Bourg I. and Sposito G. (2008). Isotopic fractionation of noble gases by diffusion
336 in liquid water: Molecular dynamics simulations and hydrologic applications.
337 *Geochim. Cosmochim. Acta* **72**, 2237–2247.

338 Brennwald, M. S., Hofer, M., Peeters, F., Aeschbach-Hertig, W., Strassmann, K.,
339 Kipfer, R., and Imboden, D. M. (2003). Analysis of dissolved noble gases in
340 the pore water of lacustrine sediments. *Limnol. Oceanogr.: Methods* **1**, 51–62.

341 Brennwald, M. S., Kipfer, R., and Imboden, D. M. (2005). Release of gas bubbles
342 from lake sediment traced by noble gas isotopes in the sediment pore water.
343 *Earth Planet. Sci. Lett.* **235**, 31–44.

344 Brennwald, M. S., Vogel, N., Scheidegger, Y., Tomonaga, Y., Livingstone, D. M.,
345 and Kipfer, R. (2013). Noble gases as environmental tracers in sediment pore
346 waters and in stalagmite fluid inclusions. In *The Noble Gases as Geochemical*
347 *Tracers*. Springer, Berlin, Heidelberg, pp. 123–153.

348 Craig H. and Gordon L. (1965). Deuterium and oxygen 18 variation in the ocean
349 and marine atmosphere. In *Stable Isotopes in Oceanographic Studies and Pa-*
350 *leotemperatures (eds. E. Tongiogi).* Spoleto, Pisa, pp. 9–130.

351 Crank, J. (1975). *The mathematics of diffusion, 2nd ed.* Clarendon Press, Oxford.

352 Cussler, E. L. (2009). *Diffusion: Mass transfer in fluid systems, 3rd ed.* Cambridge
353 Univ. Press, Cambridge.

354 Daynes, H. (1920). The process of diffusion through a rubber membrane. *Proc.*
355 *Royal Soc. London.* **97**, 286–307.

356 Graham, T. (1833). On the law of the diffusion of gases. *Philos. Mag.* **2**, 175–190,
357 269–276, 351–358.

Holocher, J., Peeters, F., Aeschbach-Hertig, W., Hofer, M., Brennwald, M. S., Kinzelbach, W., and Kipfer, R. (2002). Experimental investigations on the formation of excess air in quasi-saturated porous media. *Geochim. Cosmochim. Acta* **66**, 4103–4117.

Jähne, B., Heinz, G., and Dietrich, W. (1987a). Measurement of the diffusion coefficients of sparingly soluble gases in water. *J. Geophys. Res.* **92**, 10767–10776.

Jähne, B., Münnich, K. O., Bösinger, R., Dutzi, A., Huber, W and Libner, P. (1987b). On the parameters influencing air-water gas exchange. *J. Geophys. Res.* **92**, 2156–2202.

Kipfer, R., Aeschbach-Hertig, W., Peeters, F., and Stute, M. (2002). Noble gases in lakes and ground waters. *In Noble Gases in Geochemistry and Cosmochemistry (eds. D. Porcelli, C. J. Ballentine and R. Wieler).* Mineralogical Society of America, pp. 615–700.

Klump, S., Kipfer, R., Cirpka, O., Harvey, C., Brennwald, M. S., Ashfaque, K., Badruzzaman, A., Hug, S., and Imboden, D. M. (2006). Groundwater dynamics and arsenic mobilization in Bangladesh assessed using noble gases and tritium. *Environ. Sci. & Technol.* **40**, 243–250.

Lee, J.-Y., Marti, K., Severinghaus, J.P., Kawamura, K., Yoo, H.-S., Lee, J.B., Kim, J.S. (2006). A redetermination of the isotopic abundances of atmospheric Ar. *Geochim. Cosmochim. Acta* **70**, 4507–4512.

Lippmann, J., Stute, M., Torgersen, T., Moser, D., Hall, J., Lin, L., Borcsik, M., Bellamy, R., and Onstott, T. (2003). Dating ultra-deep mine waters with noble gases and ^{36}Cl, Witwatersrand Basin, South Africa. *Geochim. Cosmochim. Acta* **67**, 4597 – 4619.

Ludwig, R. (2001). Water: From Clusters to the Bulk. *Angewandte Chemie International Edition* **40**, 1808–1827.

Mächler, L., Brennwald, M. S., and Kipfer, R. (2012). Membrane inlet mass spectrometer for the quasi-continuous on-site analysis of dissolved gases in groundwater. *Environ. Sci. Technol.* **46**, 8288–8296.

Mark, D.F., Stuart, F.M., de Podesta, M., (2011). New high-precision measurements of the isotopic composition of atmospheric argon. *Geochim. Cosmochim. Acta* **75**, 7494–7501.

Moore, J. (1999). *Physical chemistry, 5th ed.* Prentice Hall.

Ozima, M. and Podosek, F. (2002). *Noble gas geochemistry*. Cambridge Univ. Press, Cambridge.

Pavese, F., Fellmuth, B., Head, D. I., Hermier, Y., Hill, K. D., and Valkiers, S. (2005). Evidence of a systematic deviation of the isotopic composition of neon from commercial sources compacyan with its isotopic composition in air. *Anal. Chem.* **77**, 5076–5080.

Peeters, F., Beyerle, U., Aeschbach-Hertig, W., Holocher, J., Brennwald, M. S., and Kipfer, R. (2002). Improving noble gas based paleoclimate reconstruction and groundwater dating using ^{20}Ne/^{22}Ne ratios. *Geochim. Cosmochim. Acta* **67**, 587–600.

Richter, F., Mendybaev, R., Christensen, J., Hutcheon, I., Williams, R., Sturchio, N., and Beloso Jr., A. (2006). Kinetic isotopic fractionation during diffusion of ionic species in water. *Geochim. Cosmochim. Acta* **70**, 277–289.

Schlosser, P. and Winckler, G. (2002). *Noble gases in geochemistry and cosmochemistry,* In Noble Gases in Geochemistry and Cosmochemistry (eds. D. Porcelli, C. J. Ballentine and R. Wieler). Mineralogical Society of America, pp. 701–730.

Schwarzenbach, R. P., Gschwend, P. M., and Imboden, D. M. (2003). *Environmental Organic Chemistry (2nd ed.)* New York: John Wiley & Sons, Inc.

Sun, X., Hu, Y., and Zhu, H. (2013). Ab initio potential energy surface and picted rotational spectra for the Ne–H_2O complex. *J. Chem. Phys.* **138**, 1–7.

Tempest, K. E. and Emerson, S. (2013). Kinetic isotopic fractionation of argon and neon during air-water gas transfer. *Mar. Chem.* **153**, 39 – 47.

Visser, A., Broers, H., and Bierkens, M. (2007). Dating degassed groundwater with ^{3}H/^{3}He. *Water Resour. Res.* **43**.

417 Wise, D. and Houghton, G. (1968). Diffusion coefficients of neon, krypton, xenon,
418 carbon monoxide and nitric oxide in water at 10–60 ^{o}C. *Chem. Eng. Sci.* **23**,
419 1211 – 1216.

420 Zhou, Z., Ballentine, C. J., Kipfer, R., Schoell, M., and Thibodeaux, S. (2005).
421 Noble gas tracing of groundwater coalbed methane interaction in the San Juan
422 Basin, USA. *Geochim. Cosmochim. Acta* **69**, 5413–5428.